Food and Bioproducts Processing 157 (2026) 240–251

Contents lists available at ScienceDirect

Food and Bioproducts Processing

journal homepage: www.elsevier.com/locate/fbp

Controlled carotenoid cleavage and nanoencapsulation for the production of photoprotective retinoids from *Daucus carota*

Daniel Carvajal [a], Catalina Agudelo [a], Valentina Jaramillo [a], Juan Pablo Galvis [a], Sergio González [a], Lina Trujillo [a], Karent Bravo [a], Juan Camilo Henao-Rojas [a,b], Edison Osorio [a,*]

[a] Grupo de Investigación en Sustancias Bioactivas, Facultad de Ciencias Farmacéuticas y Alimentarias, Universidad de Antioquia, Calle 70 No. 52-21, Medellín, Colombia
[b] Corporación Colombiana de Investigación Agropecuaria (AGROSAVIA), CI La Selva, Km 7 vía Rionegro-Las Palmas, Rionegro 054048, Colombia

ARTICLE INFO

Keywords:
Daucus carota
Carotenoid valorization
Oxidative cleavage
Retinoid
UV-induced oxidation
Photoprotection

ABSTRACT

This study presents an integrated strategy for the valorization of carrot (*Daucus carota* L.) processing waste through the production of photoprotective retinoid-enriched ingredients obtained via controlled carotenoid cleavage and nanoencapsulation. Carrot discards were extracted using different organic solvents, with hexane and dichloromethane yielding the highest contents of β-carotene and α-carotene. Successive extraction cycles showed a saturation-like behavior, supporting the selection of 2–4 cycles for optimal carotenoid recovery. Carotenoids were converted into apocarotenoids and retinoids using several oxidative treatments, including UV irradiation, heating, ultrasound, and air bubbling, with or without Fenton-based radical initiation. Among these, UV irradiation was the only condition that consistently generated retinoids, with yields significantly enhanced in the presence of the Fenton system. A Box–Behnken experimental design identified carotenoid concentration and irradiation time as the main factors governing degradation and retinoid formation, favoring low carotenoid loads and short exposure times to minimize secondary photodegradation. The resulting retinoid-enriched extract (RE) exhibited enhanced photoprotective activity in UVB-irradiated HaCaT keratinocytes, increasing cell viability by approximately 15–20% compared to a carotenoid extract (CE) at the highest tested concentration (5000 μg/mL). In contrast, both extracts showed comparable antioxidant and anti-inflammatory effects. To enhance stability and dermal delivery, RE was incorporated into nanostructured lipid carriers (NLCs). Optimized NLCs displayed a mean particle size of ~210 nm, high encapsulation efficiency (>99%), and a stable negative zeta potential (~−40 mV), maintaining physicochemical stability under refrigerated storage. Overall, this work demonstrates a scalable, green-compatible approach that combines controlled carotenoid cleavage with nanotechnology to obtain stable, photoprotective retinoid-enriched ingredients with potential applications in dermocosmetic formulations.

1. Introduction

Carrots (*Daucus carota* L.) are a widely cultivated crop, with global production exceeding 50 million tons annually. However, approximately 30% of the harvested carrots are discarded due to cosmetic defects, size irregularities, surface damage, oversupply, or failure to meet stringent market quality standards (Anal, 2017; Clementz et al., 2019; Râpă et al., 2024). Currently, most rejected carrots are diverted to low-value applications, such as animal feed or compost. Smaller fractions are used for the extraction of dietary fibers, resistant starch, and bioactive compounds destined for functional foods and nutraceuticals (Anal, 2017; Hussain et al., 2020). Among these valorization pathways, the extraction and transformation of bioactive compounds into high-value ingredients represents the most promising valorization strategy, given their potential application in the cosmetic and pharmaceutical industries. In the specific case of carrot waste, rejected roots —excluding those affected by spoilage— constitute a reliable and sustainable source of bioactive compounds for further processing.

Carrots contain a diverse array of bioactive compounds, including anthocyanins, phenolic acids, and carotenoids. Among commonly consumed vegetables, carrots are one of the richest natural sources of provitamin A carotenoids, particularly β-carotene—their predominant

* Corresponding author.
E-mail address: edison.osorio@udea.edu.co (E. Osorio).

https://doi.org/10.1016/j.fbp.2026.03.016
Received 28 January 2026; Received in revised form 4 March 2026; Accepted 13 March 2026
Available online 15 March 2026

carotenoid—with concentrations reported up to 30.4 mg/100 g (Ahmad et al., 2019). Although β-carotene exhibits intrinsic antioxidant and photoprotective activity (Bogacz-Radomska & Harasym, 2018; Stahl & Sies, 2012; Sereti et al., 2024), Its biological relevance in human physiology primarily derives from its enzymatic conversion into retinoids. In vertebrates, β-carotene undergoes symmetric oxidative cleavage to yield two molecules of retinol (vitamin A) (Dela Seña et al., 2016; Wang et al., 2023). α-carotene serves as an additional precursor capable of producing one retinol molecule, making carrots a highly efficient dietary source of provitamin A. Retinoids are emerging as superior photoprotective bioactives due to their ability to neutralize UV-induced reactive oxygen species (ROS) and regulate cytokine expression associated with oxidative stress and inflammation (Catanzaro et al., 2020; Ma et al., 2025; Zhong et al., 2025). By activating RAR and RXR nuclear receptors, retinoids modulate antioxidant and cell-regulatory gene expression, promote epidermal renewal, stimulate collagen synthesis, and enhance stratum corneum thickening. Furthermore, they suppress AP-1 and NF-κB pathways, ultimately reducing pro-inflammatory cytokines such as IL-6 and TNF-α (Pradhan et al., 2024). This dual antioxidant and anti-inflammatory action positions retinoids as key molecules for active photoprotection.

Although retinoids have traditionally been the primary focus of carotenoid-derived compounds, they constitute only a small fraction of the broader spectrum of oxidative cleavage products collectively known as apocarotenoids, a wide range of structures derived from carotenoid breakdown (Beltrán & Wurtzel, 2025). Carotenoids can be transformed into apocarotenoids and retinoids through several degradation pathways, including oxidation, thermal degradation, photodegradation, and free radical-mediated reactions (Harrison, 2022; Mordi et al., 2020). The process of autoxidation has also been shown to favor retinoid formation alongside other apocarotenoids (Boon et al., 2010; Rodriguez & Rodriguez-Amaya, 2007). These mechanisms differ markedly in their selectivity and reproducibility: while thermal and photodegradation often lead to extensive, non-specific breakdown of the polyene backbone, autoxidation tends to generate a more defined set of apocarotenoids, including retinoid-like molecules (Harrison, 2022; Rodriguez & Rodriguez-Amaya, 2007). Autoxidation is a spontaneous radical-driven process affecting primarily polyunsaturated molecules under atmospheric conditions (Boon et al., 2010; Rodriguez & Rodriguez-Amaya, 2007). However, despite its relevance, autoxidation remains difficult to control, as its kinetics and product profile are strongly influenced by oxygen availability, light, and temperature. This lack of selectivity and process stability currently limits its application for producing specific apocarotenoids of interest. Therefore, establishing controlled and reproducible oxidative conditions is essential to obtain enriched apocarotenoid extracts with defined composition.

On the other hand, despite the recognized photoprotective, anti-inflammatory, and anti-aging potential of apocarotenoids and retinoids, their effective action depends on the ability of the active molecules to reach deeper skin layers —particularly the dermis, where most UV-induced molecular damage occurs (Gunasekaran et al., 2014; Silva et al., 2014). However, achieving efficient dermal delivery remains challenging due to their high lipophilicity, chemical instability, and susceptibility to oxidative degradation. Nanostructured Lipid Carriers (NLCs) have emerged as a promising strategy to overcome these limitations, as their nanometric size and lipid composition can enhance cutaneous permeation and reduce transepidermal water loss through the formation of an occlusive superficial film. Moreover, NLCs can improve payload stability and enable deeper penetration with a more sustained release profile (Khan et al., 2023). Nevertheless, despite these advantages, current NLC systems have not been specifically optimized to address the intrinsic instability and oxidative reactivity of carotenoid-derived molecules. Therefore, developing nanocarrier formulations capable of simultaneously enhancing dermal delivery and protecting these highly labile actives constitutes a critical unmet need that limits their effective topical application. To address this, the present study aims to valorize carrot waste by producing a carotenoid-rich extract and establishing controlled oxidative-cleavage conditions to obtain retinoid- and retinoid-enriched ingredients. The resulting product was incorporated into a nanostructured system and evaluated in keratinocytes to assess its photoprotective potential. Achieving this requires addressing carotenoid instability, improving oxidative selectivity, and ensuring process scalability. Advances in green extraction and nanoencapsulation technologies provide a promising framework to address these challenges. Unlike previous studies that independently address carotenoid extraction or nanoencapsulation, this work integrates controlled autoxidative cleavage of carrot-derived carotenoids with targeted enrichment of retinoid-like apocarotenoids and their subsequent stabilization within a nanostructured lipid system. To our knowledge, this is the first study to combine process-controlled carotenoid oxidation with nanoencapsulation as a unified strategy for producing photoprotective retinoid-enriched ingredients from carrot waste.

2. Materials and methods

2.1. Plant material and extraction procedures

Discarded carrots (*Daucus carota* L., varieties Berlicum and Nantes), rejected due to cosmetic defects or size irregularities, were obtained from a local farm through Agrosavia (Corporación Colombiana de Investigación Agropecuaria). Fresh material was grated using a commercial food processor to obtain pieces of approximately 1 cm^2. This material was dried in a Stokes 38-B convective oven (F.J. Stokes Corporation, PHL, USA) at 40 °C for 72 h until reaching a moisture content of 5%. The dried material was milled using a commercial grain grinder (Cgoldenwall, China) and sieved through a 40-mesh screen. The resulting carrot powder was mixed with chromatographic-grade solvents (dichloromethane, hexane, tetrahydrofuran (THF), or ethanol (Merck GmbH, Darmstadt, Germany)) at a 1:4 (w/v) ratio. These suspensions were sonicated in an Elmasonic P60H ultrasound bath (Elma Schmidbauer GmbH, Germany) at 40 kHz for 20 min, and subsequently vacuum filtered. A 2 mL aliquot of each extract was transferred to plastic vials and stabilized with 100 μg/mL butylated hydroxytoluene (BHT; Sigma-Aldrich, St. Louis, MO, USA). Samples were centrifuged at 13,000 rpm for 10 min at 12 °C. For THF and ethanol extracts, 100 μL of the supernatant were directly transferred to chromatography vials. For dichloromethane and hexane extracts, 1 mL of supernatant was evaporated using a CentriVap system (Labconco Kansas City, MO, USA), reconstituted in THF containing 100 μg/mL BHT, and prepared for chromatographic analysis. All extractions were performed in triplicate; only datasets with a coefficient of variation (%CV) $<$ 10% were considered for further analysis.

2.2. Determination of carotenoids and retinoids

For the quantification of carotenoids and retinoids by HPLC-DAD, the following analytical standards were used: β-carotene (Merck GmbH, Darmstadt, Germany), retinoic acid (Tretinoin; Dr. Ehrenstorfer, Augsburg, Germany), all-trans-retinal (Sigma-Aldrich, St. Louis, MO, USA), and trans-apo-8´-carotenal (Sigma-Aldrich, St. Louis, MO, USA). For each standard, 1.0 mg was accurately weighed and dissolved in 10 mL of HPLC-grade THF containing 100 μg/mL BHT, to obtain 100 μg/mL stock solutions. Calibration curves were constructed from serial dilutions (80, 40, 20, 10, 5, and 2.5 μg/mL) prepared in HPLC vials and injected in duplicate. This procedure was performed independently on three separate occasions to ensure reproducibility. α-carotene was identified by comparison of UV-Vis spectra with library databases and quantified using the β-carotene calibration curve, with results expressed as β-carotene equivalents. All weighing operations were conducted using an AUW220D analytical balance with a precision of 0.01 mg (Shimadzu, Kyoto, Japan).

Chromatographic analyses were performed on an Agilent 1200/1260

Series HPLC System (Agilent Technologies, Santa Clara, CA, USA) equipped with a degasser module, a multigradient channel valve, a quaternary pump (G7111A), an autosampler (G1329A), a column oven (G1316A), and a diode array detector (G1315D DAD). Separation was achieved using a Develosil C30-UG Column (5 μm, 4.6 ×250 mm; Nomura Chemical, Seto, Japan). The mobile phase consisted of chromatographic-grade isopropanol (IPA) and methanol (Merck GmbH, Darmstadt, Germany), both stabilized 100 μg/mL BHT. The flow rate was set to 0.7 mL/min, the following gradient was applied: 20% IPA / 80% methanol at 0–10 min, a linear increase to 80% IPA / 20% methanol maintained until 28 min, and a return to initial conditions by 28.5 min, followed by a re-equilibration step until 35 min. The injection volume was 5 μL. Thecolumn temperature was maintained at 18 ºC. Detection wavelengths were set at 450 nm for β-carotene and apo-8´-carotenal, 350 nm for retinoic acid, and 380 nm for retinal (bandwidth: 4 nm). Chromatographic data were processed using OpenChrom software, applying the following automated commands: (i) baseline filtration (lowest intensity); (ii) subtract baseline filter; (iii) baseline filtration (SNIP); (iv) baseline subtraction; (v) peak identification (first derivative); (vi) Trapezoidal peak integration; and (vii) automatic report generation.

2.3. Oxidative cleavage of carotenoids

A factorial design was implemented to evaluate various oxidative cleavage treatments, including ultraviolet (UV) exposure, controlled heating, ultrasound, and air bubbling. Each treatment was conducted both with and without a free-radical initiator generated via the Fenton reaction. Sampling was performed at 3, 5, 7, and 10 min for all treatments. The Fenton reagent was prepared by mixing 2 mL of 30% hydrogen peroxide (Carlo Erba, Milan, Italy) with 10 mL of 10 mg/mL ferrous sulfate ($FeSO_4$; Sigma-Aldrich, MO, USA) under stirring for 15 min. To initiate oxidative cleavage, 40 mL of the dichloromethane extract (Section 2.1) were added to the reagent. The resulting mixture was then subjected to the specific cleavage conditions. For UV-induced oxidation, 15 mL of extract were transferred to a 50 mL beaker and exposed to a 365 nm handheld UV lamp (UVP, China). For ultrasound treatment, 15 mL of the sample were placed in a 50 mL Erlenmeyer flask and sonicated in a 40 kHz ultrasonic bath. For air-induced oxidation, 100 mL of extract were transferred to a 150 mL glass tube equipped with a bottom-positioned air diffuser, with airflow of 1.5 L/min. Thermal treatment was conducted by heating 15 mL of the extract in a water bath at 35 °C. Oxidative degradation was monitored by quantifying β-carotene, retinoids, and apocarotenoids using the chromatographic method described previously. BHT was added immediately after sampling to ensure reaction termination and analytical stability of carotenoid-derived products.

2.4. Optimization of UV light degradation

UV-induced oxidative cleavage was optimized using a Box–Behnken experimental design with four factors evaluated at three levels. The selected factors were: (i) Fenton reagent interphase contact time (10, 15, and 20 min); (ii) reaction volume (20, 30, and 40 mL); (iii) carotenoid concentration (5.71, 11.42, and 17.14 g/L); and (iv) incident irradiation surface area (4.72, 12.38, and 17.5 cm^2). A total of 27 experimental runs were performed (Supplementary Material, Table S1). The irradiation areas shown in this table correspond to the bottom cross-sectional areas of 10, 50, and 100 mL beakers. To standardize the irradiation distance and eliminate photon reflection, a wooden chamber was constructed with a matte black interior, ensuring that the samples were exposed exclusively to the controlled UV source.

2.5. Photoprotective effects of carotenoid and retinoid-enriched extracts in UV-irradiated human keratinocytes

The photoprotective effects of the carotenoid extract (CE) and retinoid-enriched extract (RE) were evaluated in human keratinocytes (HaCaT cells). Photoprotection was determined by assessing cell viability following UV irradiation, alongside the modulation of key markers associated with inflammation and oxidative stress —namely interleukin 6 (IL-6) production and intracellular reactive oxygen species (ROS) levels.

2.5.1. Cell viability

The assays were performed using immortalized human keratinocytes (HaCaT) obtained from the Cell Bank of San Vicente de Paul Hospital (Medellín-Colombia). Cells between passages 42 and 46 were used for all experiments. HaCaT cells were maintained in Dulbecco's Modified Eagle Medium (DMEM) supplemented with 10% fetal bovine serum (FBS) and 1% penicillin-streptomycin, and cultured at 37 °C in a humidified atmosphere containing 5% CO_2. For viability assays, cells were seeded in 96-well plates at a density of 1×10^4 cells per well and allowed to adhere overnight. Subsequently, cells were treated with increasing concentrations of the CE or the RE, at concentrations ranging from 1.31 to 5000 μg/mL, prepared via two-fold serial dilutions from a 100 mg/mL stock solution in DMSO. The final concentration of DMSO in the culture medium was kept constant across all treatments and did not exceed the level previously validated as non-cytotoxic under the experimental conditions. The effect of DMSO alone on cell viability was evaluated in preliminary control experiments, confirming that the selected concentration had no statistically significant impact on HaCaT viability. DMEM supplemented with 1% penicillin–streptomycin was used as the dilution medium. After 24 h of treatment, cell viability was assessed using the MTT assay. Briefly, MTT solution (5 mg/mL) was added to each well to achieve a final concentration of 0.5 mg/mL, followed by incubation for 3 h at 37 °C. The supernatant was then removed, and the resulting formazan crystals were solubilized in DMSO. Absorbance was measured at 570 nm using a multi-mode microplate reader (BioTek Instruments, Inc., USA). Cell viability was expressed as a percentage relative to untreated control cells.

2.5.2. Protective effect against UVB-induced cell death

The photoprotective effect of the samples against UVB-induced cytotoxicity was evaluated using immortalized human HaCaT keratinocytes. A toxic UVB dose (80 mJ/cm^2) was applied to induce cell death in approximately 40–60% of the cell population and to assess whether the treatment conferred protection against UVB-induced damage. To evaluate the prophylactic effect, samples were applied prior to irradiation. For the assays, HaCaT cells were seeded in 96-well plates at a density of 1×10^4 cells per well in 100 μL of supplemented medium and allowed to adhere overnight. The medium was then removed, and cells were treated with the test samples for 24 h. Samples were evaluated at the same concentration range used in the cell viability assay (1.31–5000 μg/mL), using DMEM supplemented with 1% penicillin–streptomycin as the diluent. After treatment, the medium containing the samples was removed, and cells were washed with phosphate-buffered saline (PBS). Fresh medium supplemented with 1% penicillin–streptomycin was then added, and cells were irradiated with UVB at a dose of 80 mJ/cm^2 using a UV Irradiation System for Cultures (Vilber Lourmat, Marne-la-Vallée, France). Following irradiation, cells were incubated for an additional 24 h at 37 °C. Cell viability was subsequently determined using the MTT assay, as described above. Absorbance was measured at 570 nm using a multi-mode microplate reader (BioTek Instruments, Inc., USA). Cell viability was expressed as a percentage relative to untreated and non-irradiated control cells. A photoprotective effect was defined as treatments that resulted in significantly higher cell viability compared to the irradiated control.

2.5.3. Measurement of intracellular reactive oxygen species (ROS)

Intracellular ROS production in HaCaT keratinocytes was induced by UVA irradiation (2.5 J/cm^2) and quantified using the fluorescent probe 2′,7′-dichlorofluorescein diacetate (DCFDA; Molecular Probes Inc., Eugene, OR, USA), following established procedures (Castañeda et al., 2023). The effect of the CE and the RE on ROS generation was evaluated using a 24 h pre-treatment protocol at concentrations of 2, 20, 200, and 2,000 μg/mL. For the assay, HaCaT cells were seeded in black 96-well plates at a density of 5 × 10^4 cells per well in supplemented medium and allowed to adhere overnight at 37 °C in a humidified atmosphere containing 5% CO_2. The medium was then removed, and cells were treated with the extracts for 24 h. Following treatment, cells were washed with phosphate-buffered saline (PBS), and 100 µL of 2′, 7′-dichlorodihydrofluorescein diacetate (H_2DCFDA, 25 μM) prepared in PBS were added to each well. Plates were incubated for 30 min at 37 °C in the dark. Subsequently, cells were irradiated with UVA at a dose of 2.5 J/cm^2, and fluorescence was measured immediately at excitation/emission wavelengths of 485/516 nm using a Synergy HT multi-mode microplate reader (BioTek Instruments, Inc., USA) maintained at 37 °C. Quercetin (25 μM) was used as a positive antioxidant control. Results were expressed as the percentage of fluorescence relative to the irradiated control.

2.5.4. Modulation of the inflammatory biomarker IL-6

Interleukin-6 (IL-6) production in HaCaT keratinocytes following UVB irradiation was evaluated as a marker of the inflammatory response using an enzyme-linked immunosorbent assay (ELISA). IL-6 levels were quantified using a DuoSet ELISA kit (R&D Systems, Minneapolis, MN, USA) according to the manufacturer's instructions. Cells were seeded in 96-well plates at a density of 1 × 10^4 cells per well and incubated overnight at 37 °C in a humidified atmosphere containing 5% CO_2. After adhesion, the culture medium was removed, and cells were pre-treated for 24 h with CE or RE at concentrations of 2, 20, 200, and 2000 μg/mL. Following treatment, the cells were washed with PBS, fresh medium containing 1% penicillin-streptomycin was added, and the cells were irradiated with UVB at a dose of 60 mJ/cm^2. Cells were then incubated for an additional 24 h. After incubation, culture supernatants were collected, and IL-6 concentrations were determined by ELISA according to the manufacturer's protocol. Results were expressed relative to the irradiated control.

2.5.5. Statistical analysis

All results are expressed as the mean ± standard deviation (SD) from at least three independent experiments, each performed in triplicate. Statistical analyses were carried out using GraphPad Prism version 5.0 (GraphPad Software Inc., San Diego, CA, USA). Differences among groups were assessed by one-way analysis of variance (ANOVA), followed by Dunnett's multiple comparison test to compare treated groups with the corresponding control. Differences were considered statistically significant at $p < 0.05$.

2.6. Formulation and optimization of Nanostructured Lipid Carriers (NLCs)

2.6.1. Lipid screening

The solubility of the RE was first evaluated in six liquid lipids (linseed oil, jojoba oil, sacha inchi oil, castor oil, oleic acid, and medium-chain triglycerides) by mixing the extract at 10% w/w with each lipid. Solubility was assessed via visual inspection. Subsequently, the solubility of RE in four solid lipids (cocoa butter, Compritol® 888 ATO, glyceryl monostearate, and beeswax) was screened. For this, the extract (10% w/w) was incorporated into binary blends of each solid lipid and the previously selected liquid lipid at ratios of 2:1, 7:3, and 10:1 (w/w). The resulting lipid melts were evaluated visually and microscopically immediately after preparation. To assess the presence or absence of extract crystals within the solidified lipid melts, samples were examined under a Leitz Orthoplan microscope (Wetzlar, Germany).

2.6.2. Preparation of nanolipid carriers

NLCs were prepared by ultrasonication following the method described previously with minor modifications (Brugè et al., 2013). The retinoid-enriched extract (RE) was first dissolved in the selected liquid lipid. The solid lipid was then melted at a temperature 2 °C above its melting point, and the liquid lipid phase was incorporated. This molten lipid phase was dispersed into the hot aqueous phase (maintained 5 °C above the lipid temperature) using a high-speed homogenizer (Ultra--Turrax T25, IKA-Werke GmbH & Co. KG, Staufen, Germany) at 12000 rpm for 2 min to obtain a pre-emulsion. This mixture was subsequently ultrasonicated using a 21-mm probe (LSP-500, Industrial Sonomechanics, New York, USA) at 40% amplitude for 70 s, applying a pulse cycle of 10 s ON and 10 s OFF; during this process, the dispersión was kept in an ice bath to prevent the temperature from exceeding 80 °C. The lipid phase was formulated using a liquid-to-solid lipid ratio of 3:7. Additional formulations were prepared using two natural surfactants and evaluated independently. Final NLC dispersions contained 0.05% RE, 6% total lipid phase, 2% surfactant, and 0.5% preservative (w/w).

2.6.3. Particle size and zeta potential characterization

Mean particle size and size distribution (polydispersity index, PDI) were determined by Dynamic Light Scattering (DLS), using a Zetasizer Nano ZS90 (Malvern Instruments, Malvern, UK). Measurements were conducted at 25°C with a fixed scattering angle of 90°. Samples were diluted in deionized water to avoid multiple-scattering effects, and the refractive index was set to match that of the continuous phase. The zeta potential (ζ) was measured by electrophoretic light scattering using the instrument's M3-PALS mode (Phase Analysis Light Scattering). ζ -potential values were automatically calculated from the electrophoretic mobility using the Smoluchowski model.

2.6.4. Encapsulation efficiency (%EE)

Encapsulation efficiency (%EE) was determined by quantifying the concentration of free extract in the dispersion medium and the total extract in the formulation. Extract concentration was measured spectrophotometrically at 359 nm (λmax) using a microplate reader (BioTek Instruments, Inc., USA). The free extract was obtained by separating non-encapsulated compounds from the NLC dispersion using Vivaspin® 500 centrifugal concentrators (Sartorius, Germany) with a 3 kDa molecular weight cut-off (MWCO) membrane. Approximately 500 mg of NLCs dispersion were placed in the upper chamber, and the filtrate containing the free extract was collected after centrifugation at 13,000 rpm for 5 h. To determine the total extract content, ~250 mg of NLCs dispersion were mixed with 1000 μL of extraction solvent (hexane–methanol–acetone, 2:1:1 v/v/v, containing 2.5% BHT) and 1000 μL of saponification solution (water–methanol–20% KOH in methanol, 1:1:1 v/v/v). The supernatant was transferred to a 2.0 mL volumetric flask, and a second extraction was performed. The supernatants were combined and adjusted to the final volume. The encapsulation efficiency (%EE) was calculated using the following equation:

$$\%EE = \frac{\text{Total extract} - \text{Free extract}}{\text{Total extract}} \times 100 \text{Equation } N°1$$

2.6.5. Experimental design to optimize the RE-Loaded Lipid Nanocarrier

Table S2, provided in the Supplementary Material, summarizes the experimental design used to optimize the encapsulation of the apocarotenoid-rich extract in the nanostructured lipid system. Lipid percentage and surfactant percentage were selected as independent variables at two levels (low and high). The response variables evaluated were %EE, particle size, and zeta potential. Three central points were included to estimate pure error. Data analysis was performed using STATISTICA 10.0®.

2.6.6. Stability studies

The optimized formulation was stored in amber glass containers to protect it from light, environmental humidity, and contamination. Physical and chemical stability were evaluated over a 30-day period at two different storage conditions: refrigeration (4 °C ± 0.5 °C) and room temperature (21 °C ± 5° C; 60% ± 5% relative humidity). Stability was evaluated after 7, 14, and 30 days through visual inspection and the monitoring of %EE, particle size, and zeta potential.

3. Results and discussion

3.1. Higher carotenoid yields with nonpolar solvents and saturation behavior across enrichment cycles

The organic solvents evaluated showed marked differences in their ability to extract α- and β-carotene (Fig. 1A). Ethanol showed the lowest extraction capacity (61.43 μg/mL), whereas hexane and dichloromethane achieved the highest yield (169.42 and 166.84 μg/mL, respectively), followed by THF (116.82 μg/mL). These results are consistent with polarity-dependent solubilization trends; however, carotenoid extraction efficiency is not governed exclusively by solvent polarity. Additional factors such as solvent–matrix interactions, lipid co-extraction, carotenoid molecular structure, and mass transfer dynamics likely contribute to the observed differences, as previously reported for plant-derived carotenoid systems (Chuyen et al., 2017). In addition, the extraction efficiencies of hexane and dichloromethane were not statistically different. Despite its comparable performance, dichloromethane presents well-recognized toxicological and regulatory limitations that may restrict its applicability in food or cosmetic contexts. Therefore, its use in this study should be understood as a laboratory-scale comparative solvent, while industrial translation would require consideration of safer and regulatory-compliant alternatives. Regarding the enrichment cycles (Fig. 1B), the extraction profile displayed a saturation-like behavior characterized by diminishing gains with each successive cycle. Although both linear and logarithmic models were evaluated, the logarithmic model showed a better fit to the data ($R^2 = 0.8835$) compared to the linear model. While this coefficient indicates a moderate level of explained variance, the model captures a nonlinear trend with an apparent inflection between cycles 2 and 4, corresponding to the stage where the most pronounced increases in carotenoid concentration were observed when sequential extraction was applied. This pattern reflects a progressive enrichment driven by repeated solvent–solute re-equilibration, while indicating that additional cycles beyond this range contribute minimally to yield. Thus, limiting extraction to cycles 2–4 maximizes carotenoid recovery while maintaining process efficiency, offering a rational basis for defining operational conditions during scale-up.

3.2. Enrichment of retinoid formation by UV-driven cleavage

Carotenoid oxidation can generate a broad spectrum of cleavage products, and previous studies indicate that the oxidizing agent strongly influences which apocarotenoids are preferentially formed (Boon et al., 2010; Rodriguez & Rodriguez-Amaya, 2007). Based on this, four analytical responses were defined for each treatment: (i) carotenoid degradation (α-carotene and β-carotene); (ii) retinoid formation (retinoic acid and retinal); (iii) apo-8´-carotenal formation; and (iv) α- and β-ionone formation. These responses provide mechanistic insight into the cleavage pathways activated under each condition and support the optimization of treatments aimed at maximizing the concentration of bioactive oxidation products. Carotenoid degradation results showed that UV irradiation was the most effective treatment, both with and without the Fenton initiator (Fig. 2). The presence of the initiator further enhanced degradation but only when combined with UV exposure, reaching values above 60%. The observed linear trend suggests that extended exposure times could further increase degradation efficiency. In contrast, some treatments exhibited negative degradation values, suggesting an apparent increase in carotenoid concentration. While this effect does not necessarily reflect de *novo* formation, it may arise from the enhanced release or solubilization of carotenoids that were previously entrapped within the plant matrix. This phenomenon aligns with recent reports demonstrating that the disruption of cellular structures can increase carotenoid recoverability (Han et al., 2024; Priscilla et al., 2024).

Ultrasound, air bubbling, and thermal exposure treatments —whether applied alone or combined with the Fenton initiator —failed to produce quantifiable amounts of retinoids. In contrast, UV irradiation promoted a clear increase in retinoid formation, rising from 6.5 to ~8.5 μg/mL in the UV-only treatment and from 5 to > 11 μg/mL when combined with the Fenton system after 10 min. This behavior is consistent with the photochemical susceptibility of polyene chains, where UV photons induce *cis–trans* isomerization and homolytic cleavage, leading to short-chain apocarotenoids and retinoid-like molecules (Boon et al., 2010). The further enhancement observed in the presence

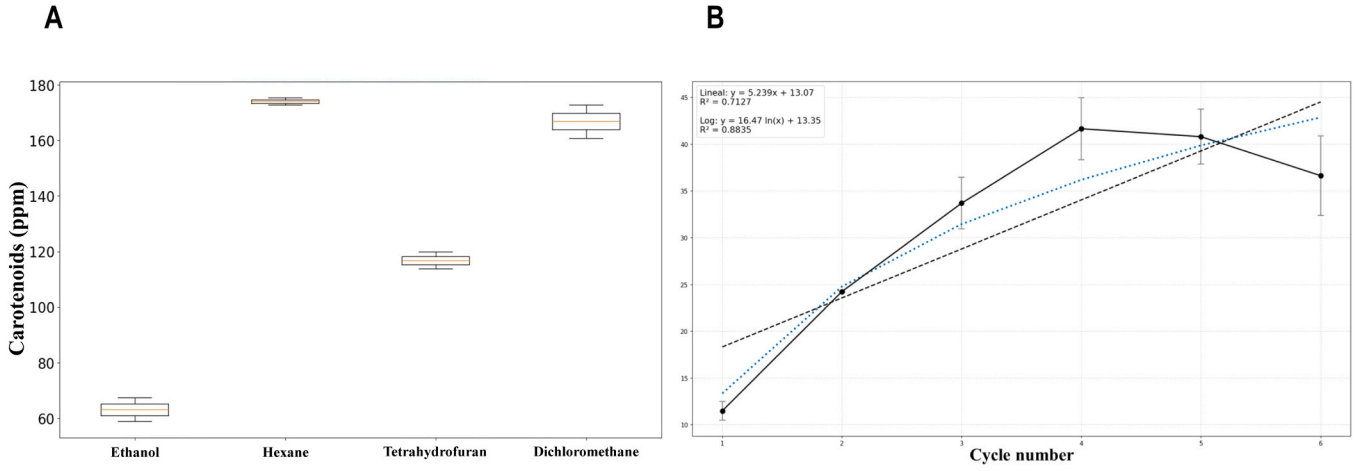

Fig. 1. Solvent-dependent carotenoid extraction efficiency and enrichment behavior across successive extraction cycles. (A) Yield of total carotenoids (α- and β-carotene) obtained with four organic solvents—ethanol, tetrahydrofuran (THF), dichloromethane, and hexane—using a 1:4 (w/v) extraction ratio. Bars represent mean ± SD of triplicate extractions (n = 3). (B) Enrichment of total carotenoids across successive extraction cycles. Data represent mean ± SD of three independent replicates. Carotenoid quantification for both panels was performed by HPLC–DAD using external calibration with β-carotene and expressed as β-carotene equivalents.

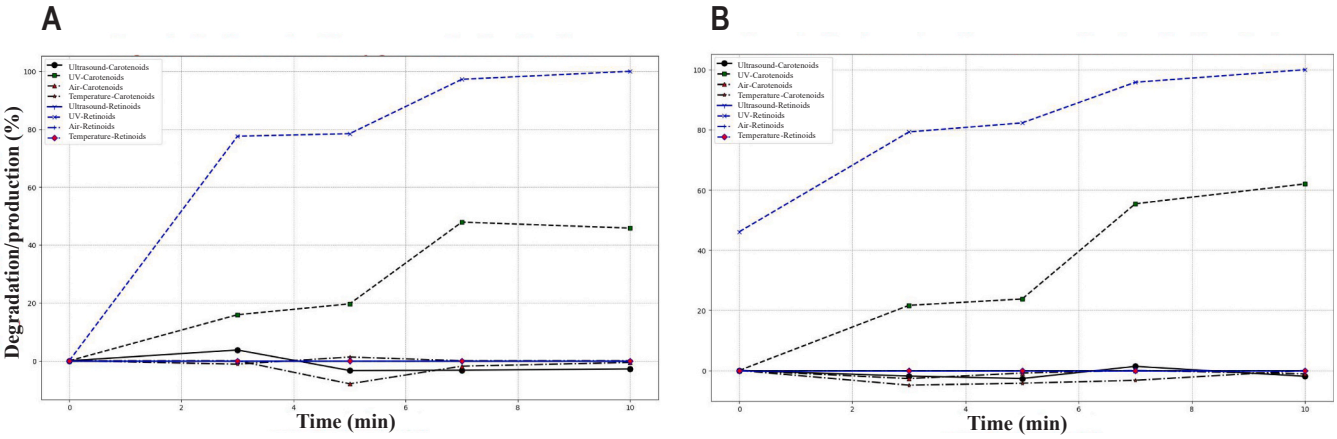

Fig. 2. Kinetics of carotenoid degradation and retinoid formation under four oxidative treatments. (A) Carotenoid degradation and retinoid production in the absence of Fenton initiator for ultraviolet irradiation (365 nm), ultrasound (40 kHz), air bubbling (1.5 L/min), and thermal exposure (35 °C). (B) Effect of incorporating a Fenton radical initiator ($FeSO_4/H_2O_2$) on the same oxidative treatments. Data represent mean ± SD of three independent replicates (n = 3). Different letters denote statistically significant differences ($p < 0.05$) between treatments at each time point (one-way ANOVA followed by Tukey's test).

of the Fenton system reflects the hydroxyl radical–driven acceleration of oxidative scission (Mordi et al., 2020; Rodriguez & Rodriguez-Amaya, 2007). Notably, under the experimental conditions evaluated, no detectable levels of apo-8′-carotenal or α/β-ionone were observed, which may reflect a relative enrichment of cleavage pathways contributing to retinoid formation. Conversely, the lack of retinoid formation in the other treatments is consistent with their limited energy input and lower radical availability. Together, these results confirm that photochemical activation, particularly when assisted by controlled radical generation, provides the most effective pathway for producing retinoid-rich extracts from carotenoids.

3.3. UV light optimization using Box–Behnken design

Given that UV irradiation produced the highest carotenoid degradation and retinoid formation among all evaluated treatments, this condition was selected for optimization using a Box–Behnken response surface design. The experimental matrix, presented in Supplementary Material (Table S1), evaluated the combined effects of four factors: Fenton interphase time, reaction volume, carotenoid concentration, and irradiation area, on two key responses: the percentage of carotenoid degradation (sum of α-carotene and β-carotene) and the percentage of retinoid generation (sum of retinoic acid and retinal). The experimental data were fitted to a quadratic polynomial model including linear, quadratic, and interaction terms. To assess the relative influence of each factor on both responses, a forest plot summarizing standardized regression coefficients is presented in Fig. 3. This analysis enabled the identification of the optimal conditions that most effectively promote the conversion of carotenoids into retinoids under UV-driven oxidative cleavage.

The quadratic regression analysis revealed that only a subset of the evaluated factors exerted statistically significant effects on the experimental responses. In the forest plots, significant effects correspond to coefficients whose confidence intervals do not cross zero, while non-significant factors exhibit intervals spanning the $\beta = 0$ axis. For carotenoid degradation, the dominant factor was carotenoid concentration, as evidenced by the magnitude and significance of both its linear and quadratic terms (Fig. 3A). Lower concentrations (4 g/L) markedly increased degradation, whereas higher concentrations (12 g/L) suppressed it, aligning with the trends observed in Supplementary Material

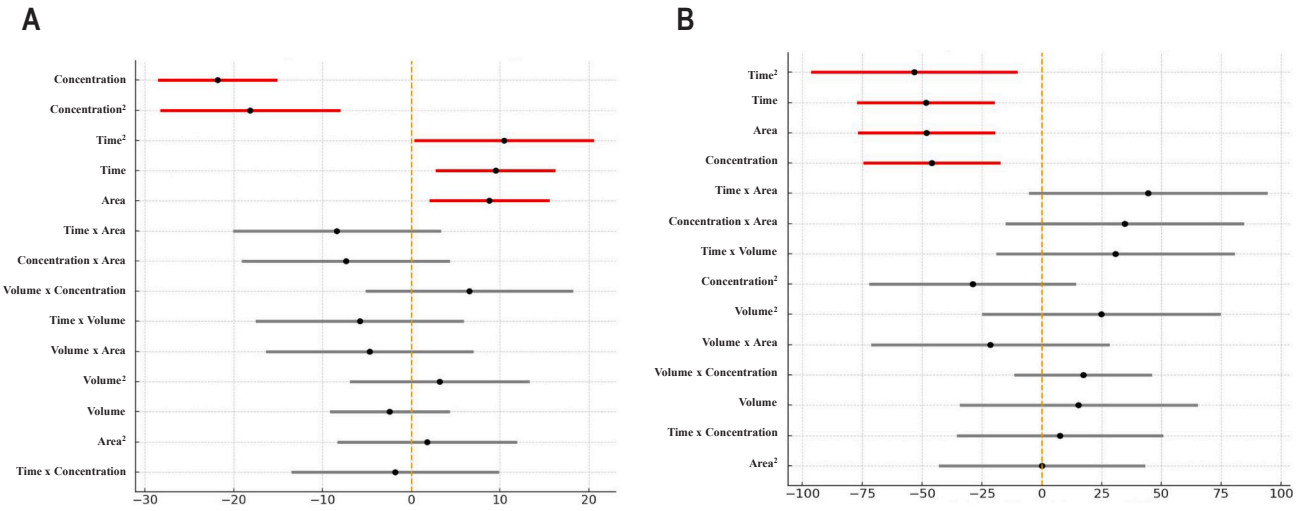

Fig. 3. Standardized regression coefficients from the Box–Behnken response-surface model for UV-induced (A) carotenoid degradation, and (B) retinoid formation. Positive coefficients indicate factor levels that increase the response, whereas negative coefficients indicate inhibitory effects. Bars represent the magnitude and direction of each term (linear, quadratic, and interaction) in the fitted multiple-regression model. All coefficients correspond to the experimental matrix shown in Supplementary Table S2 and were estimated from three independent replicates per treatment condition.

(Table S1). This inverse relationship may be attributed to increased turbidity at higher concentrations, which reduces photon penetration and limits photochemical cleavage. In contrast, reaction volume showed no significant effect. Both irradiation area and Fenton interphase time exhibited positive but modest contributions, indicating that broader irradiation surfaces and longer radical-generation times enhance degradation, although their effect sizes are substantially smaller than that of concentration. Notably, none of the interaction terms was statistically significant.

Regarding retinoid formation, all significant coefficients in Fig. 3B were negative, indicating that increasing concentration, irradiation area, or reaction time negatively impacts retinoid yield. These trends likely reflect the dual role of UV exposure: while it promotes carotenoid scission, it simultaneously may accelerate the secondary photodegradation of newly formed retinoids, which are intrinsically more photolabile than their precursors. Additionally, higher carotenoid concentrations, though already associated with lower degradation efficiency, also reduce retinoid formation due to limited precursor conversion. Taken together, these findings indicate that low carotenoid concentrations and controlled, shorter irradiation times are critical for maximizing retinoid generation while minimizing secondary degradation. Consequently, these parameters should be prioritized in subsequent kinetic studies and process optimization efforts.

3.4. Photoprotective effects, intracellular ROS modulation, and IL-6 production in UV-irradiated HaCaT cells

The photoprotective potential of CE and RE was evaluated in UV-irradiated keratinocytes by assessment of cell viability, intracellular reactive oxygen species (ROS) production, and interleukin-6 (IL-6) secretion. A clear differentiation between the formulations was observed primarily in the photoprotective endpoint. RE demonstrated superior protection against UVB-induced cytotoxicity at elevated concentrations ($\geq$ 500 μg/mL), reaching approximately 15–20% higher cell viability than CE at the highest tested dose (5000 μg/mL; Fig. 4A). Although these photoprotective effects were observed at comparatively elevated concentrations, such levels remain within the functional range commonly employed for topical antioxidant and photoprotective actives, supporting their biological relevance while emphasizing the need for optimized delivery strategies to enhance efficacy at lower doses (Mukherjee et al., 2006). This concentration-dependent advantage is consistent with the well-documented role of retinoids in regulating keratinocyte survival, differentiation, and epidermal homeostasis through nuclear receptor–mediated pathways, although direct activation of these mechanisms was not evaluated in the present study. At lower and intermediate concentrations (1.31–200 μg/mL), both extracts conferred comparable protection, suggesting that the intrinsic antioxidant capacity of carotenoids is sufficient to provide basal photoprotection within this dose range. In contrast, intracellular ROS suppression and modulation of IL-6 secretion revealed limited differentiation between CE and RE. Both extracts attenuated UVA-induced ROS production across the tested concentration range (2–2000 μg/mL), with comparable maximal reductions observed at the highest concentrations (Fig. 4B). These findings indicate that antioxidant activity under acute oxidative stress conditions is largely driven by shared or overlapping mechanisms, such as direct radical scavenging and modulation of cellular redox balance, rather than retinoid enrichment. Similar patterns have been reported for complex plant-derived extracts, where multiple constituents contribute synergistically to ROS modulation (Villanueva-Bermejo et al., 2024). Regarding UVB-induced IL-6 production (Fig. 4C), both extracts reduced cytokine levels at low concentrations, while CE exhibited a more pronounced inhibitory effect at intermediate doses. No consistent enhancement associated with RE was observed across the concentration range evaluated. This non-linear response suggests that inflammatory modulation is primarily mediated by carotenoid-associated mechanisms and may not benefit from retinoid enrichment under the experimental conditions employed. Such endpoint-specific behavior underscores the complexity of inflammatory signaling in keratinocytes and highlights that cytoprotection, oxidative stress modulation, and cytokine regulation do not necessarily follow identical dose–response patterns.

The differential use of UVA and UVB radiation further supports these observations. UVA radiation (320–400 nm) predominantly induces indirect photo-oxidative damage via ROS generation, making it a suitable model for evaluating antioxidant effects, whereas UVB radiation (280–320 nm) primarily affects the epidermis, causing direct DNA damage, reduced cell viability, and activation of pro-inflammatory pathways such as NF-κB and AP-1, which promote IL-6 synthesis (D'Orazio et al. 2013; Pfeifer, 2020; Gromkowska-Kępka et al. 2021; Ansary et al., 2021). Collectively, these results indicate a stratified biological response: retinoid enrichment selectively enhances protection against acute UVB-induced cell death at high concentrations, whereas antioxidant and anti-inflammatory effects are comparable between CE and RE or, in the case of IL-6 modulation, favor CE at intermediate doses. This differential behavior highlights the importance of extract composition and biological endpoint selection when defining functional applications. While RE appears particularly suited for high-intensity photoprotective strategies aimed at preserving keratinocyte viability, its limited advantage at lower concentrations may be associated with the intrinsic instability of retinoids, their susceptibility to photodegradation, and restricted cellular bioavailability. In this context, nanotechnology-based delivery systems—such as lipid nanoparticles, nanoemulsions, or polymeric carriers—represent a promising approach to enhance retinoid stability, improve cellular uptake, and potentiate

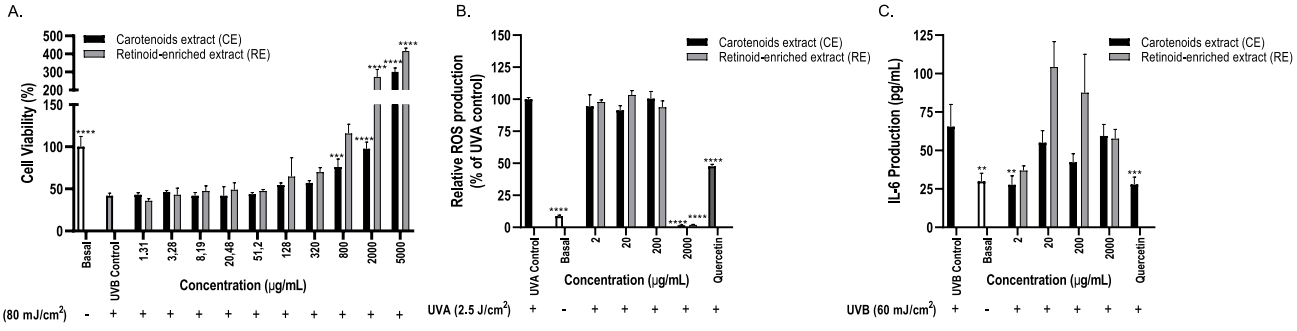

Fig. 4. Photoprotective effects of carotenoid extract (CE, black bars) and retinoid-enriched extract (RE, grey bars) on UV-induced damage in HaCaT keratinocytes. Cells were pre-treated for 24 h, the extracts were removed, and cells were exposed to the UV radiation specified in each panel. (A) Cell viability assessed by MTT assay; (B) Intracellular ROS levels measured by DCFDA; (C) IL-6 production quantified by ELISA. Data are expressed as mean ± SD of three independent experiments. Statistical significance was determined by one-way ANOVA followed by Dunnett's test versus the irradiated control (**$p < 0.01$, ***$p < 0.001$, ****$p < 0.0001$). Bars without asterisks indicate no significant differences.

photoprotective efficacy at reduced doses, supporting the future development of RE-based dermocosmetic or photoprotective formulations.

3.5. Performance and optimization outcomes of retinoid-loaded NLCs

3.5.1. Lipid screening and rational selection of formulation components

To rationally design stable NLCs capable of encapsulating highly labile retinoid-derived compounds, an initial lipid screening was performed to identify excipients compatible with the physicochemical properties of the RE. Although the extract was initially soluble in all tested liquid lipids, formulations containing linseed, jojoba, and castor oils developed a dark precipitate after 24 h, suggesting limited long-term compatibility. In contrast, medium-chain triglycerides ensured stable solubilization over time, supporting their selection as the liquid lipid phase due to their defined composition and established use in nanostructured lipid carriers. Considering that compound solubility decreases upon lipid solidification, potentially leading to phase separation and expulsion from the lipid matrix (Xia et al., 2007), solid lipid screening was conducted. While no macroscopic crystals were detected, microscopic analysis revealed that cocoa butter and beeswax yielded homogeneous dispersions with uniformly distributed extract domains (Fig. 5). These solid lipids were therefore selected for nanocarrier formulation. Final formulation optimization was guided by achieving a nanometric particle size (~186 nm), homogeneous consistency, and physical stability for at least one month. Among the evaluated surfactants, a plant-derived amphiphilic system composed primarily of lipids and amino acids was selected due to its high epidermal biocompatibility and intrinsic pH within the physiological skin range, eliminating the need for pH adjustment and reducing the risk of destabilization associated with acidic or basic additives (Romeo et al., 2024).

3.5.2. Experimental design to optimize the retinoid-loaded NLCs

Fig. 6 summarizes the statistical evaluation of the formulation variables on particle size, encapsulation efficiency (%EE), and zeta potential. The Pareto analysis (Fig. 6A) revealed that lipid percentage was the only factor exerting a statistically significant effect on particle size, confirming the critical role of lipid and surfactant composition in controlling the dimensions of NLCs. Consistent with previous reports, increased lipid content - particularly liquid lipids - and low surfactant-to-lipid ratios tend to generate larger particles, whereas higher surfactant proportions favor size reduction by stabilizing the lipid–aqueous interface (Haider et al., 2020). Response surface analysis for particle size (Fig. 6B) indicated a moderate model fit ($R^2 = 75.5\%$), although the model was not statistically significant overall ($p = 0.1208$). Nevertheless, a clear linear effect of lipid and surfactant percentages was observed, with no evidence of curvature or factor interaction. In contrast, both %EE and zeta potential remained largely insensitive to compositional changes within the explored ranges, reflected by the low predictive power of their respective models ($R^2 = 45.65\%$ and 33.58%). Consequently, particle size emerged as the only response exhibiting a defined and interpretable trend, suggesting that broader formulation ranges may be required to adequately model the remaining responses. Based on these findings, a desirability analysis (Supplementary Material, Fig. 1) was conducted to optimize the formulation toward a reduced particle size (180–220 nm), high encapsulation efficiency (70–100%), and a sufficiently negative zeta potential (≤ -30 mV) (Santinon et al., 2023). As expected, optimization was predominantly driven by particle size minimization, leading to optimal formulation at 6.03% lipid and 2.5% surfactant (global desirability = 0.73). The resulting NLCs exhibited a mean particle size of 209.8 nm, a narrow polydispersity index (PDI < 0.3), a highly negative surface charge (~ −40 mV), and nearly complete extract encapsulation (99.6%). These characteristics are particularly favorable for topical delivery; particle size and homogeneity are critical determinants of skin penetration, as smaller and monodisperse systems enhance contact with the stratum corneum, increase specific surface area, and promote efficient delivery of apocarotenoids such as retinol (Weber et al., 2014).

3.5.3. Stability evaluation of retinoid-loaded NLCs formulations

The stability study evaluated the influence of temperature and storage time on the physicochemical properties of the nanocarriers. After 30 days, all samples exhibited an increase in viscosity, while slight

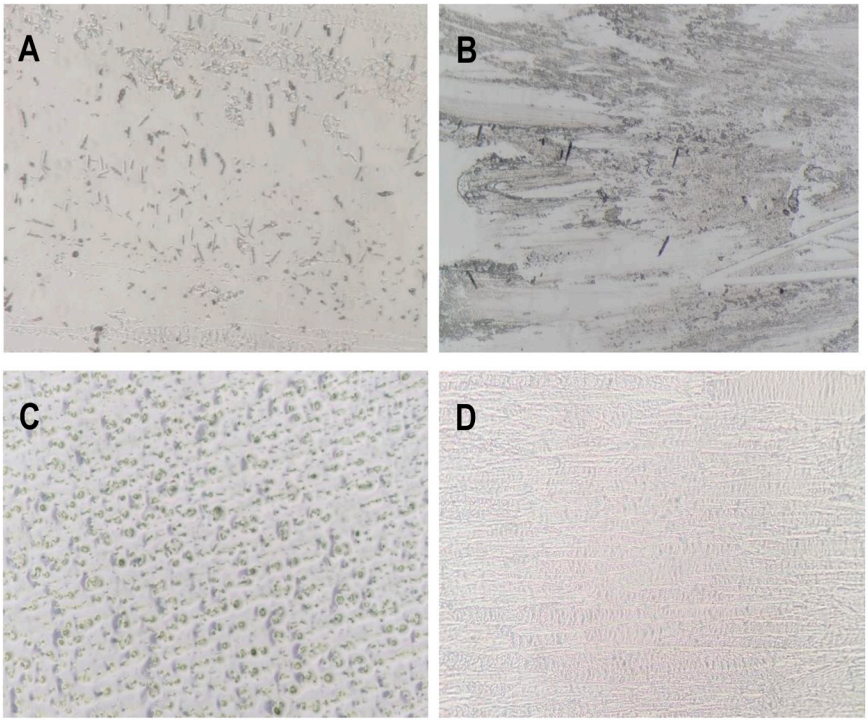

Fig. 5. Light microscope pictures of lipid films with 10% of retinoid-enriched extract. A) Compritol ATO 888-LL (7:3); B) Glyceryl monostearate-LL (10:1); C) Cocoa butter-LL (7:3), D) Beewax-LL (10:1).

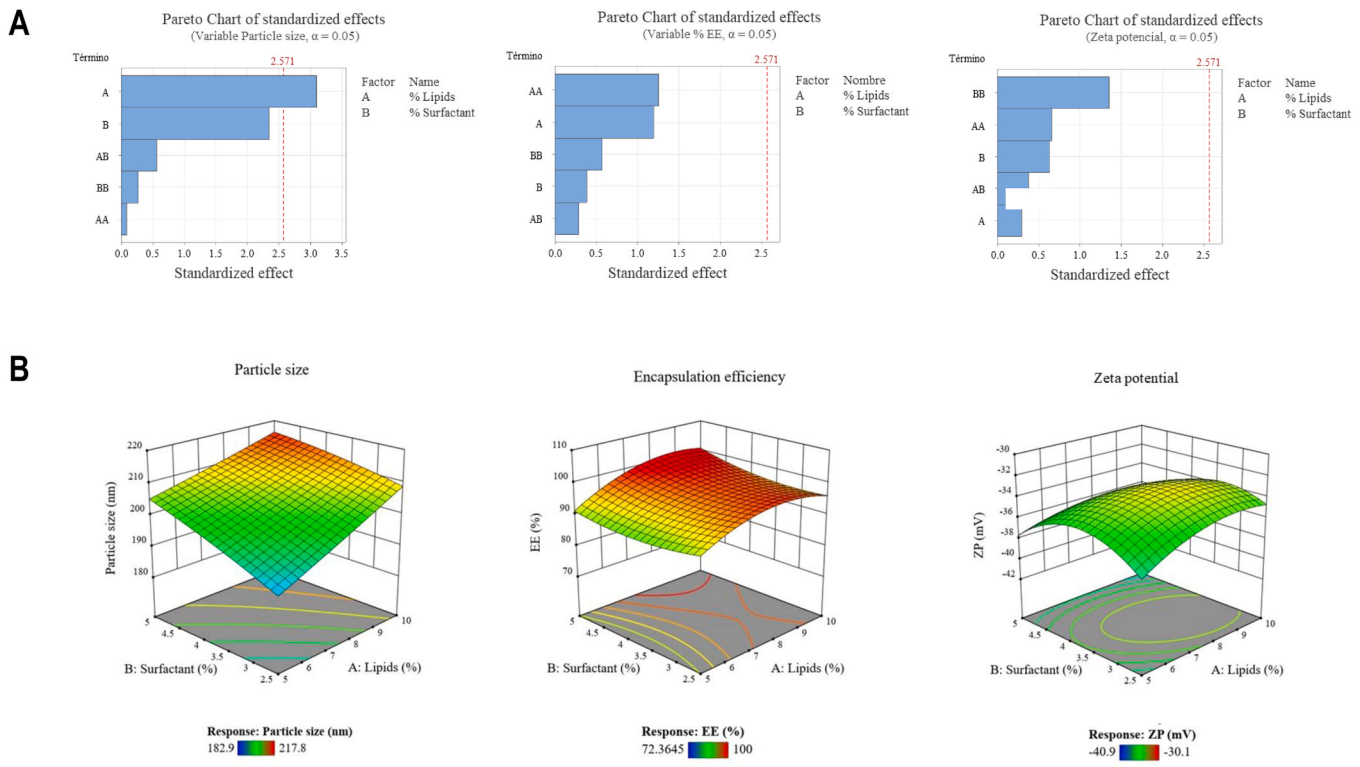

Fig. 6. Statistical analysis of formulation variables influencing particle size, encapsulation efficiency (%EE), and zeta potential: (A) Pareto chart at 95% confidence interval; (B) response surface plot.

discoloration occurred only under ambient conditions. These visual changes aligned with a more pronounced decline in encapsulation efficiency at room temperature (Fig. 7A), although the values remained within an acceptable range (>70%) (Ferreira et al., 2020). This behavior agrees with the intrinsic tendency of nanodispersions to evolve toward thermodynamically more stable states, often resulting in particle growth over time (Rahmasari et al., 2022). Particle size analysis confirmed this growth during the first 14 days at room temperature (Fig. 7B). However, at later time points, and particularly under refrigeration, a progressive reduction in particle size was observed. Although uncommon, this trend is theoretically feasible and may arise from kinetically driven mechanisms such as internal structural reorganization, component loss, or surface degradation (Chauhan et al., 2020; Houacine et al., 2020; Pornputtapitak et al., 2024; Schroder et al., 2025). Regarding colloidal stability, the zeta potential remained below the –30 mV threshold for most of the study (Fig. 7C), supporting sustained electrostatic repulsion. Nonetheless, the appearance of aggregates on the final day coincided with the lowest zeta potential values, indicating weakened repulsive forces and the onset of particle association (Haider et al., 2020).

The stability profile of the encapsulated extract over time is illustrated in Fig. 8. Initially, NLCs formulations (represented by the blue and green lines) exhibited values near unity (ranging from 0.95 to 0.98 at time point 1), suggesting that the lipid matrix provides robust initial protection for the encapsulated compounds. Although a gradual decline was observed over the 30-day monitoring period, the formulations retained approximately 60% of their original content (fold change ~0.60). These findings align with the observations of Charoenputtakhun et al. (2014), who noted that the stability of all-trans retinoic acid (ATRA) in lipid nanoparticles is highly temperature-dependent, with optimal retention (>80%) occurring at 4 °C. The observed degradation in this study may be related to the structural modifications of the lipid matrix; as emphasized in the literature, optimizing lipid composition is crucial to prevent the expulsion of active ingredients caused by polymorphic transitions during storage (Morales et al., 2015; Teeranachaideekul et al., 2007).

To evaluate the stability of the encapsulated extract relative to its unencapsulated counterpart over time, a control gel containing 0.5% free extract was formulated and maintained under storage conditions identical to those of the prepared NLCs. Statistical analysis via a paired *t*-test indicated significant differences, confirming the enhanced stability

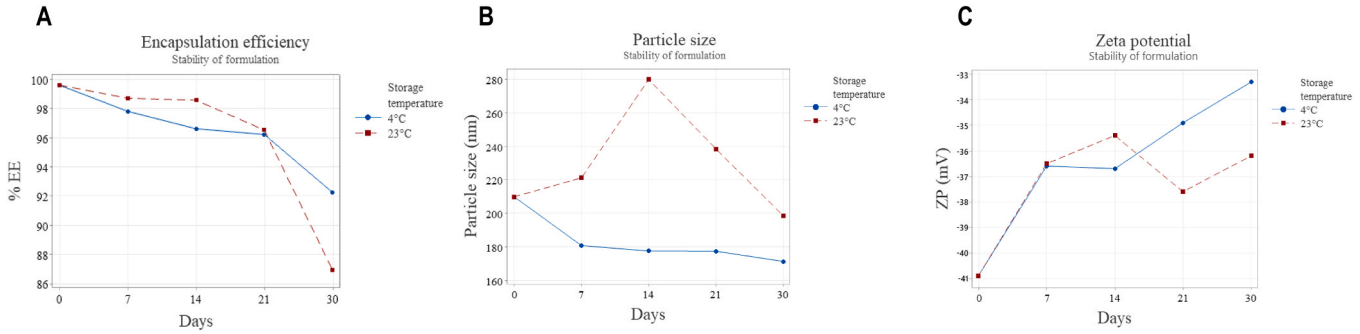

Fig. 7. Stability study of NLCs. A) Encapsulation efficiency. B) Particle size. C) Zeta potencial.

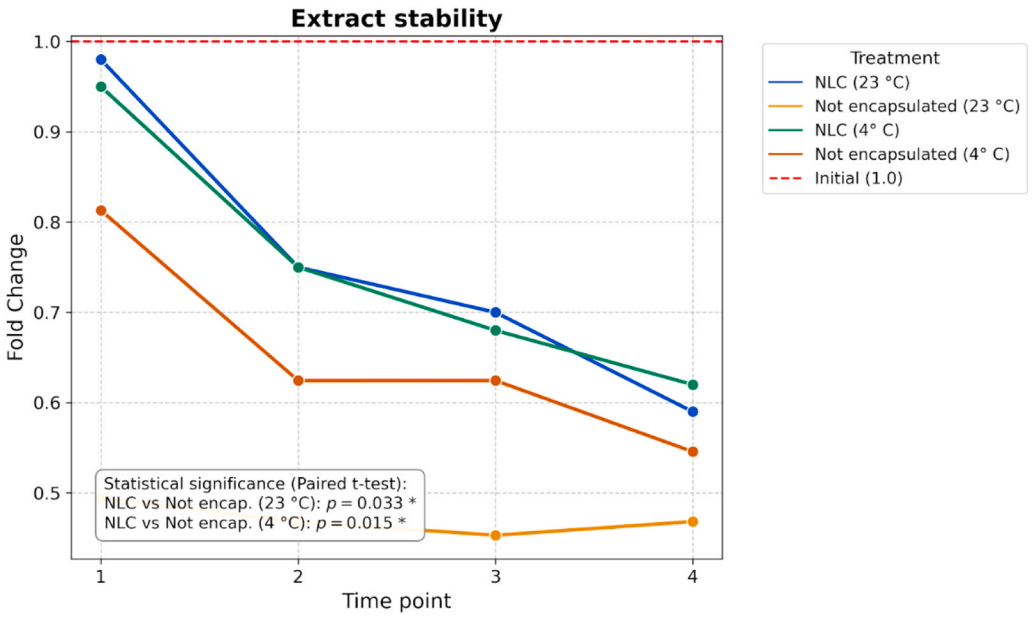

Fig. 8. Stability of encapsulated versus non-encapsulated retinoid-rich extract (RE). Paired Student's t-test; (*) indicates statistical significance ($p < 0.05$).

provided by the NLCs matrix at both 23 °C ($p < 0.05$) and 4 °C ($p < 0.05$). While all formulations exhibited a certain degree of degradation, NLCs encapsulation effectively mitigated the rapid decline observed in the free extract.

Several studies have demonstrated that the primary function of retinoids encapsulated in nanostructured lipid carriers (NLCs) lies in their ability to provide controlled and sustained release, thereby optimizing the therapeutic response and reducing side effects compared to conventional administration routes, while also serving as an effective strategy to overcome their high chemical instability (Morales et al., 2015). For instance, tretinoin-loaded NLC formulations, developed via probe sonication using stearic and oleic acids, have yielded nanometric particles (~762 nm) with an entrapment efficiency exceeding 94% (Ghate et al., 2016). Regarding all-trans retinoic acid (ATRA), chemical stability has proven to be highly dependent on the lipid matrix composition, achieving optimal preservation under refrigeration (4 °C) (Charoenputtakhun et al., 2014). In the same study, the physical stability of these carriers was heavily influenced by the oil phase; notably, NLCs formulated with medium-chain triglycerides (MCT) maintained a constant particle size (121–192 nm) over 30 days regardless of storage temperature. Furthermore, advanced methods such as vacuum emulsification have facilitated the synthesis of uniform-sized retinol nanocarriers (VLN-ROL, <200 nm), which protect the active ingredient from oxidative degradation, enhance its dermal delivery by a factor of 2.2, and significantly reduce skin irritation (Jun et al., 2021). Additionally, NLCs formulated with Precirol ATO 5 and oleic acid have proven effective for the targeted delivery of adapalene (third-generation retinoid) to pilosebaceous units, leveraging their small particle size (~173 nm) for deep follicular penetration (Ahmad-Nasrollahi et al., 2021).

To the best of our knowledge, published research has primarily focused on the encapsulation of pure retinoid derivatives; the encapsulation of complex extracts containing such molecules remains unexplored. Nevertheless, our results are comparable to those reported for pure compounds in terms of the obtained particle size and encapsulation efficiency. The lipid nanoparticles proposed in this study demonstrate significant potential as a delivery vehicle for a retinoid-enriched carrot extract intended for topical formulations. However, these findings underscore the need to optimize the formulation to achieve greater long-term stability, as well as to direct future research toward evaluating dermal penetration, release profiles, and the mitigation of adverse effects associated with the encapsulated actives.

4. Conclusions

This study demonstrates that the controlled oxidation of carotenoids enables the generation of extracts with distinct chemical profiles and differentiated biological activities in human keratinocytes exposed to UV radiation. While both the CE and the RE exhibited photoprotective, antioxidant, and anti-inflammatory effects, their biological responses were endpoint- and concentration-dependent. Retinoid enrichment selectively enhanced protection against UVB-induced cytotoxicity at high concentrations, suggesting a specific role for retinoids in promoting keratinocyte survival under acute UV stress. In contrast, antioxidant activity and modulation of UVB-induced IL-6 production were comparable between extracts or favored CE at intermediate concentrations, indicating that these effects are primarily driven by carotenoid-associated mechanisms. Together, these findings highlight the functional specialization of carotenoid- and retinoid-rich fractions and underscore the importance of extract composition when evaluating photoprotective efficacy. Moreover, the results support the potential of retinoid-enriched extracts as active ingredients for applications targeting epidermal resilience to UV damage, while also pointing to the need for formulation strategies, such as nanotechnology-based delivery systems, to enhance retinoid stability and bioavailability for improved performance at lower doses.

CRediT authorship contribution statement

Valentina Jaramillo: Methodology, Investigation. **Juan Pablo Galvis:** Methodology, Investigation. **Daniel Carvajal:** Writing – original draft, Validation, Methodology, Investigation. **Catalina Agudelo:** Writing – original draft, Methodology, Investigation. **Edison Osorio:** Writing – review & editing, Writing – original draft, Supervision, Resources, Conceptualization. **Gonzalez Sergio:** Investigation, Methodology. **Karent Bravo:** Validation, Methodology, Investigation. **Juan Camilo Henao-Rojas:** Resources, Investigation, Funding acquisition. **Lina Trujillo:** Supervision, Methodology, Investigation.

Declaration of Competing Interest

The authors declare the following financial interests/personal

relationships which may be considered as potential competing interests: Edison Osorio reports financial support was provided by University of Antioquia. If there are other authors, they declare that they have no known competing financial interests or personal relationships that could have appeared to influence the work reported in this paper.

Acknowledgments

The authors express their deep appreciation to the Science, Technology, and Innovation Fund of the Sistema General de Regalias (SGR) of Colombia for supporting this research through the project "Fortalecimiento de la cadena productiva de la zanahoria mediante la generación de prototipos de productos innovadores en el Oriente del departamento de Antioquia" (code BPIN: 2020000100192). We also extend our gratitude to the University of Antioquia and the Colombian Agricultural Research Corporation (Agrosavia) for their invaluable contributions. The dedication of their researchers and the availability of institutional resources played a fundamental role in the development of this study.

Supporting information

Supplementary Material data associated with this article can be found in the online version.

Appendix A. Supporting information

Supplementary data associated with this article can be found in the online version at doi:10.1016/j.fbp.2026.03.016.

Data availability

Data will be made available on request.

References

Ahmad-Nasrollahi, S., Koohestani, F., Naeimifar, A., Samadi, A., Vatanara, A., Firooz, A., 2021. Preparation and evaluation of adapalene nanostructured lipid carriers for targeted drug delivery in acne. Dermatol. Ther. 34 (2), e14777. https://doi.org/10.1111/dth.14777.

Ahmad, T., Cawood, M., Iqbal, Q., Ariño, A., Batool, A., Tariq, R.M.S., Azam, M., Akhtar, S., 2019. Phytochemicals in *Daucus carota* and their health benefits-review article. Foods 8 (9), 424. https://doi.org/10.3390/foods8090424.

Anal, A., 2017. Food processing by-products and their utilization. John Wiley & Sons, Inc, Chichester, UK.

Ansary, T.M., Hossain, Md.R., Kamiya, K., Komine, M., Ohtsuki, M., 2021. Inflammatory molecules associated with ultraviolet radiation-mediated skin aging. Int. J. Mol. Sci. 22 (8), 3974. https://doi.org/10.3390/ijms22083974.

Beltrán, J., Wurtzel, E.T., 2025. Carotenoids: resources, knowledge, and emerging tools to advance apocarotenoid research. Plant Sci. 350, 112298. https://doi.org/10.1016/j.plantsci.2024.112298.

Bogacz-Radomska, L., Harasym, J., 2018. β-Carotene-properties and production methods. Food Qual. Saf. 2 (2), 69–74. https://doi.org/10.1093/fqsafe/fyy004.

Boon, C.S., McClements, D.J., Weiss, J., Decker, E.A., 2010. Factors influencing the chemical stability of carotenoids in foods. Crit. Rev. Food Sci. Nutr. 50 (6), 515–532. https://doi.org/10.1080/10408390802565889.

Brugè, F., Damiani, E., Puglia, C., Offerta, A., Armeni, T., Littarru, G.P., 2013. Nanostructured lipid carriers loaded with CoQ10: effect on human dermal fibroblasts under normal and UVA-mediated oxidative conditions. Int. J. Pharm. 455 (1-2), 348–356. https://doi.org/10.1016/j.ijpharm.2013.06.075.

Castañeda, C., Bravo, K., Cortes, N., Bedoya, J., de Borges, W.S., Bastida, J., Osorio, E., 2023. Amaryllidaceae alkaloids in skin cancer management: photoprotective effect on human keratinocytes and anti-proliferative activity in melanoma cells. J. Appl. Biomed. 21, 36–47. https://doi.org/10.32725/jab.2023.004.

Catanzaro, E., Bishayee, A., Fimognari, C., 2020. On a beam of light: photoprotective activities of the marine carotenoids astaxanthin and fucoxanthin in suppression of inflammation and cancer. Mar. Drugs 18 (11), 544. https://doi.org/10.3390/md18110544.

Charoenputtakhun, P., Opanasopit, P., Rojanarata, T., Ngawhirunpat, T., 2014. All-trans retinoic acid-loaded lipid nanoparticles as a transdermal drug delivery carrier. Pharm. Dev. Technol. 19 (2), 164–172. https://doi.org/10.3109/10837450.2013.763261.

Chauhan, I., Yasir, M., Verma, M., Singh, A.P., 2020. Nanostructured Lipid Carriers: a groundbreaking approach for transdermal drug delivery. Adv. Pharm. Bull. 10 (2), 150–165. https://doi.org/10.34172/apb.2020.021.

Chuyen, H.V., Roach, P.D., Golding, J.B., Parks, S.E., Nguyen, M.H., 2017. Optimisation of extraction conditions for recovering carotenoids and antioxidant capacity from Gac peel using response surface methodology. Int. J. Food Sci. Technol. 52 (4), 972–980. https://doi.org/10.1111/ijfs.13361.

Clementz, A., Torresi, P.A., Molli, J.S., Cardell, D., Mammarella, E., Yori, J.C., 2019. Novel method for valorization of by-products from carrot discards. LWT 100, 374–380. https://doi.org/10.1016/j.lwt.2018.10.085.

Dela Seña, C., Sun, J., Narayanasamy, S., Riedl, K.M., Yuan, Y., Curley, R.W., Schwartz, S.J., Harrison, E.H., 2016. Substrate specificity of purified recombinant chicken β-carotene 9′,10′-Oxygenase (BCO2). J. Biol. Chem. 291 (28), 14609–14619. https://doi.org/10.1074/jbc.M116.723684.

D'Orazio, J., Jarrett, S., Amaro-Ortiz, A., Scott, T., 2013. UV radiation and the skin. Int. J. Mol. Sci. 14 (6), 12222–12248. https://doi.org/10.3390/ijms140612222.

Ferreira, R., Napoli, J., Enver, T., Bernardino, L., Ferreira, L., 2020. Advances and challenges in retinoid delivery systems in regenerative and therapeutic medicine. Nat. Commun. 11 (1), 4265. https://doi.org/10.1038/s41467-020-18042-2.

Ghate, V.M., Lewis, S.A., Prabhu, P., Dubey, A., Patel, N., 2016. Nanostructured lipid carriers for the topical delivery of tretinoin. Eur. J. Pharm. Biopharm. 108, 253–261. https://doi.org/10.1016/j.ejpb.2016.07.026.

Gromkowska-Kępka, K.J., Puścion-Jakubik, A., Markiewicz-Żukowska, R., Socha, K., 2021. The impact of ultraviolet radiation on skin photoaging - review of *in vitro* studies. J. Cosmet. Dermatol. 20 (11), 3427–3431. https://doi.org/10.1111/jocd.14033.

Gunasekaran, T., Haile, T., Nigusse, T., Dhanaraju, M.D., 2014. Nanotechnology: an effective tool for enhancing bioavailability and bioactivity of phytomedicine. Asian Pac. J. Trop. Biomed. 4, S1–S7. https://doi.org/10.12980/APJTB.4.2014C980.

Haider, M., Abdin, S.M., Kamal, L., Orive, G., 2020. Nanostructured Lipid Carriers for delivery of chemotherapeutics: a review. Pharmaceutics 12 (3), 288. https://doi.org/10.3390/pharmaceutics12030288.

Han, K.N., Meral, H., Demirdöven, A., 2024. Recovery of carotenoids as bioactive compounds from peach pomace by an eco-friendly ultrasound-assisted enzymatic extraction. J. Food Sci. Technol. 61, 2354–2366. https://doi.org/10.1007/s13197-024-06001-4.

Harrison, E.H., 2022. Carotenoids, β-apocarotenoids, and retinoids: the long and the short of It. Nutrients 14, 1411. https://doi.org/10.3390/nu14071411.

Houacine, C., Adams, D., Singh, K.K., 2020. Impact of liquid lipid on development and stability of trimyristin nanostructured lipid carriers for oral delivery of resveratrol. J. Mol. Liq. 316, 113734. https://doi.org/10.1016/j.molliq.2020.113734.

Hussain, S., Jõudu, I., Bhat, R., 2020. Dietary fiber from underutilized plant resources-A positive approach for valorization of fruit and vegetable wastes. Sustainability 12 (13), 5401. https://doi.org/10.3390/su12135401.

Jun, S.H., Kim, H., Lee, H., Song, J.E., Park, S.G., Kang, N.G., 2021. Synthesis of retinol-loaded lipid nanocarrier via vacuum emulsification to improve topical skin delivery. Polym. (Basel) 13 (5), 826. https://doi.org/10.3390/polym13050826.

Khan, S., Sharma, A., Jain, V., 2023. An overview of nanostructured lipid carriers and its application in drug delivery through different routes. Adv. Pharm. Bull. 13 (3), 446–460. https://doi.org/10.34172/apb.2023.056.

Ma, Y., Li, C., Su, W., Sun, Z., Gao, S., Xie, W., Zhang, B., Sui, L., 2025. Carotenoids in skin photoaging: unveiling protective effects, molecular insights, and safety and bioavailability frontiers. Antioxidants 14 (5), 577. https://doi.org/10.3390/antiox14050577.

Morales, J.O., Valdés, K., Morales, J., Oyarzun-Ampuero, F., 2015. Lipid nanoparticles for the topical delivery of retinoids and derivatives. Nanomedicine 10 (2), 253–269. https://doi.org/10.2217/nnm.14.159.

Mordi, R.C., Ademosun, O.T., Ajanaku, C.O., Olanrewaju, I.O., Walton, J.C., 2020. Free radical mediated oxidative degradation of carotenes and xanthophylls. Molecules 25, 1038. https://doi.org/10.3390/molecules25051038.

Mukherjee, S., Date, A., Patravale, V., Korting, H.C., Roeder, A., Weindl, G., 2006. Retinoids in the treatment of skin aging: an overview of clinical efficacy and safety. -48 Clin. Interv. Aging 1 (4), 327. https://doi.org/10.2147/ciia.2006.1.4.327.

Pfeifer, G.P., 2020. Mechanisms of UV-induced mutations and skin cancer. Genome Instab. Dis. 1 (3), 99–113. https://doi.org/10.1007/s42764-020-00009-8.

Pornputtapitak, W., Thiangjit, Y., Tantirungrotechai, Y., 2024. Effect of functional groups in lipid molecules on the stability of Nanostructured Lipid Carriers: experimental and computational investigations. ACS Omega 9 (9), 11012–11024. https://doi.org/10.1021/acsomega.4c00685.

Pradhan, S.J., Kuchekar, A., Gawade, A., Kore, S., 2024. Retinoids - A unique ingredient for skin rejuvenation employing novel drug delivery systems. J. Appl. Pharm. Sci. 14 (07), 29–44. https://doi.org/10.7324/JAPS.2024.168608.

Priscilla, K., Sharma, V., Gautam, A., Gupta, P., Dagar, R., Kishore, V., Kumar, R., 2024. Carotenoid extraction from plant tissues. Methods Mol. Biol. 2788, 3–18. https://doi.org/10.1007/978-1-0716-3782-1_1.

Rahmasari, D., Rosita, N., Soeratri, W., 2022. Physicochemical characteristics, stability, and irritability of Nanostructured Lipid Carrier system stabilized with different surfactant ratios. J. Farm. Ilmu Kefarmasian Indones. 9 (1), 8–16. https://doi.org/10.20473/jfiki.v9i12022.8-16.

Răpă, M., Darie-Niță, R.N., Coman, G., 2024. Valorization of fruit and vegetable waste into sustainable and value-added materials. Waste 2 (3), 258–278. https://doi.org/10.3390/waste2030015.

Rodriguez, E.B., Rodriguez-Amaya, D.B., 2007. Formation of apocarotenals and epoxycarotenoids from β-carotene by chemical reactions and by autoxidation in model systems and processed foods. Food Chem. 101 (2), 563–572. https://doi.org/10.1016/j.foodchem.2006.02.015.

Romeo, M., Hafidi, Z., Muzzalupo, R., Pons, R., García, M.T., Mazzotta, E., Pérez, L., 2024. Antimicrobial and anesthetic niosomal formulations based on amino acid-

derived surfactants. Molecules 29 (12), 2843. https://doi.org/10.3390/molecules29122843.
Santinon, C., Beppu, M.M., Vieira, M.G.A., 2023. Optimization of kappa-carrageenan cationization using experimental design for model-drug release and investigation of biological properties. Carbohydr. Polym. 308, 120645. https://doi.org/10.1016/j.carbpol.2023.120645.
Schroder, R., Ozuguzel, U., Du, Y., Corts, T.M., Liu, Y., Mittal, S., Templeton, A.C., Chaudhuri, B., Gindy, M., Wagner, A., Su, Y., 2025. Molecular dynamics of lipid nanoparticles explored through solution and solid-state NMR spectroscopy and MD simulations. J. Phys. Chem. B. 129 (25), 6200–6219. https://doi.org/10.1021/acs.jpcb.5c01399.
Sereti, F., Alexandri, M., Papadaki, A., Papapostolou, H., Kopsahelis, N., 2024. Carotenoids production by *Rhodosporidium paludigenum* yeasts: Characterization of chemical composition, antioxidant and antimicrobial properties. J. Biotechnol. 386, 52–63. https://doi.org/10.1016/j.jbiotec.2024.03.011.
Silva, P., Bonifácio, B., Ramos, M., Negri, K., Maria Bauab, T., Chorilli, M., 2014. Nanotechnology-based drug delivery systems and herbal medicines: a review. Int. J. Nanomed. 9, 1–15. https://doi.org/10.2147/IJN.S52634.
Stahl, W., Sies, H., 2012. β-Carotene and other carotenoids in protection from sunlight. Am. J. Clin. Nutr. 96 (5), 1179S–1184S. https://doi.org/10.3945/ajcn.112.034819.
Teeranachaideekul, V., Müller, R.H., Junyaprasert, V.B., 2007. Encapsulation of ascorbyl palmitate in nanostructured lipid carriers (NLC)–effects of formulation parameters on physicochemical stability. Int. J. Pharm. 340 (1-2), 198–206. https://doi.org/10.1016/j.ijpharm.2007.03.022.
Villanueva-Bermejo, D., Siles-Sánchez, M., Hernández, D.M., García-Risco, M.R., Jaime, L., Santoyo, S., Fornari, T., 2024. Theoretical framework to evaluate antioxidant synergistic effects from the coextraction of marjoram, rosemary and parsley. Food Chem. 437, 137919. https://doi.org/10.1016/j.foodchem.2023.137919.
Wang, Y., Gan, S., Luo, C., Liu, T., Zhao, X., Ma, J., Lin, C., Shu, D., Qu, H., 2023. Variations in BCO2 coding sequence causing a difference in carotenoid concentration in the skin of chickens. Genes 14 (3), 671. https://doi.org/10.21203/rs.3.rs-54013/v1.
Weber, S., Zimmer, A., Pardeike, J., 2014. Solid Lipid Nanoparticles (SLN) and Nanostructured Lipid Carriers (NLC) for pulmonary application: a review of the state of the art. Eur. J. Pharm. Biopharm. 86 (1), 7–22. https://doi.org/10.1016/j.ejpb.2013.08.013.
Xia, Q., Saupe, A., Müller, R.H., Souto, E.B., 2007. Nanostructured lipid carriers as novel carrier for sunscreen formulations. Int. J. Cosmet. Sci. 29 (6), 473–482. https://doi.org/10.1111/j.1468-2494.2007.00410.x.
Zhong, J., Liang, L., Zhao, N., Wang, J., Shu, P., 2025. Synergistic effects of retinol and retinyl palmitate in alleviating UVB-induced DNA damage and promoting the homologous recombination repair in keratinocytes. Front. Pharm. 16, 1562244. https://doi.org/10.3389/fphar.2025.1562244.